Ab initio study of the downfolded self-energy for correlated systems: Momentum dependence and effects of dynamical screening

R. Sakuma,[1] C. Martins,[2,3,4] T. Miyake,[2] and F. Aryasetiawan[1]

[1]*Department of Physics, Division of Mathematical Physics, Lund University, Sölvegatan 14A 223 62 Lund, Sweden*

[2]*Nanosystem Research Institute "RICS," AIST, Tsukuba 305-8568, Japan*

[3]*Centre de Physique Théorique, Ecole Polytechnique, CNRS UMR 7644, 91128 Palaiseau Cedex, France*

[4]*CEA, DAM, DIF, Arpajon F-91297, France*

(Received 23 October 2013; revised manuscript received 27 May 2014; published 18 June 2014)

The electronic structure of strongly correlated systems is usually calculated by using an effective model Hamiltonian with a small number of states and an effective on-site interaction. The mode, however, neglects the frequency dependence of the interaction, which emerges as a result of dynamical screening processes not included in the model. The self-energy calculated in this kind of model within dynamical mean-field theory (DMFT) is usually assumed to contain on-site components only. To study the validity of model calculations for the simulation of realistic materials, we make a detailed comparison between the downfolded self-energy in a model Hamiltonian with static and dynamic on-site interaction and the full *ab initio* self-energy for Fe and $SrVO_3$ within the GW approximation. We find that the model GW self-energy shows weaker $\mathbf{k}$ (momentum) dependence than the *ab initio* GW self-energy, which is attributed to the lack of the long-range interaction and of contributions from other electrons not included in the models. This weak $\mathbf{k}$ dependence is found to lead to an artificial narrowing of the quasiparticle band structure. Moreover, this band narrowing is stronger for the dynamic (frequency-dependent) interaction, due to a larger renormalization of the quasiparticle states. These findings indicate a crucial role of the $\mathbf{k}$ dependence of the self-energy and dynamical screening for the electronic structure of correlated systems. We also discuss the effects beyond the GW approximation for correlated systems by comparing the GW and DMFT results.

DOI: 10.1103/PhysRevB.89.235119 PACS number(s): 71.20.−b, 71.27.+a

I. INTRODUCTION

Over the last decade there has been significant progress in the electronic structure calculations of strongly correlated materials owing to the successful merging of first-principles band-structure methods and lattice Fermion model approaches. One of the most important areas of progress in this field is the development of dynamical mean-field theory (DMFT) [1], which can treat strong intra-atomic interactions between localized orbitals by mapping the lattice model to an effective impurity problem. Starting from low-energy effective models whose parameters may be determined from first principles, this method offers a way to compute not only the one-particle Green's function and the self-energy but also the response functions of real correlated materials at a reasonable computational cost [2–4].

In order to construct more realistic models, works have been done to include two important factors missing in conventional models such as the Hubbard model: one is the dynamical (frequency-dependent) aspect of the screened interaction U [5], and the other is the long-range interaction. Only recently the frequency dependence of U has begun to be included in DMFT calculations [6–8], thanks to the development of new impurity solvers which can handle frequency-dependent interactions [9–11]. Related to the long-range interaction, recently it was found [12,13] that the $\mathbf{k}$ (momentum) dependence of the self-energy plays an important role in determining the electronic structure of correlated materials within the GW approximation (GWA) [14–16], although the relation between the *ab initio* calculation and low-energy model calculation was not yet investigated.

The frequency dependence of U and its long-range component influence each other in a subtle way. A static U is relatively short ranged and it is therefore reasonable to assume that only on-site U is important. On the other hand, a frequency-dependent U varies in range greatly depending on energy. At low energy below the plasmon energy, the Coulomb interaction is strongly screened so that an on-site assumption may be valid but at high energy above the plasmon energy, the screening effect is suddenly reduced so that U becomes very long range, approaching the bare Coulomb interaction. Clearly, a model with a frequency-dependent U ought to take into account the long-range nature of U at high energy.

The purpose of this paper is to investigate how the two factors, namely, the frequency dependence and long-range component of U, affect the electronic structure of the correlated systems. For this purpose, we make a detailed comparison between the self-energy and quasiparticle band structure in the *ab initio* calculation and in the low-energy effective models within the GWA. We also make a comparison between the GW and DMFT self-energies. The effective models are built with an on-site interaction, which is either static or dynamic. We show that both factors are indeed important in determining the electronic structure of correlated systems; due to the lack of a long-range component of U and the correlations with the electrons not included in the models, the self-energy in the on-site-only models exhibits a weaker momentum dependence than the *ab initio* self-energy. We also show that neglecting the frequency dependence of U results in smaller renormalization effects of the correlated states. These factors affect the bandwidth of these correlated systems in opposite directions, and the overall effect amounts to a reduction of the

bandwidth compared with the *ab initio GW* results by ≈30% for frequency-dependent interaction and ≈10%–20% for static interaction. In this work we choose spin-unpolarized Fe and $SrVO_3$ as test materials, which have been widely studied in the literature [8,17–28], but we believe the results obtained in this work are general for various correlated materials with localized states. We also make a comparison between the GW and DMFT self-energy in the static U model in order to investigate vertex corrections or correlation effects in DMFT beyond the GWA.

This paper is structured as follows: Section II outlines the downfolded self-energy in first-principles and effective low-energy models with static and dynamic interaction. Section III compares the self-energy in *ab initio* and model calculations within the GWA. In Sec. IV we discuss the correlation beyond the GWA by comparing GW and DMFT results in the static model, and in Sec. V we present our conclusions.

II. THEORY

A. Effective self-energy for correlated systems from first principles

In electronic structure calculations of strongly correlated systems, one is usually interested in only a small number of localized states near the Fermi energy. These states, such as the d orbitals of $3d$ systems, are assumed to be the most relevant for the studied correlation problem and an effective model is then built and solved in the Hilbert subspace spanned by them and therefore denoted as "d" space.

Within such an approach, one actually divides the complete Hilbert space into two subspaces: the d space which comprises the localized states of interest and the other containing the rest ("r" space) of the one-particle Hilbert space. In Ref. [29], a rigorous approach based on Hedin's equations is provided for building low-energy effective models from the full many-body Hamiltonian: By integrating out the r degrees of freedom, the full Green's function of the d electrons, G^d, can be related to the noninteracting Green's function for the d electrons, G_0^d, via a Dyson's equation as

$$G^d(1,2) = G_0^d(1,2) + \int d(34) G_0^d(1,3)\Sigma^{\text{eff}}(3,4)G^d(4,2), \tag{1}$$

where the numbers denote both space and time coordinates, i.e., $1 = (x_1, y_1, z_1, t_1)$.

Following Ref. [29], we introduce in Eq. (1) the downfolded self-energy Σ^{eff} of the electrons in the d space. This effective self-energy consists of not only the term due to correlations between the localized electrons in the d space but also a term due to correlations between the electrons in the d and r spaces. More precisely, the effective self-energy Σ^{eff} consists of the following three parts [29]:

$$\Sigma^{\text{eff}} = \Sigma^d + \Sigma^{rd} + \Sigma^{\text{drd}}, \tag{2}$$

where Σ^d is due to the correlations between the d electrons and therefore corresponds to the self-energy calculated within the effective low-energy model. On the contrary, the additional two terms cannot be caught within the effective model description: Σ^{rd} describes the contribution from electrons in the r space acting on the d space, and Σ^{drd} comes from the hybridization between d and r spaces. The last term Σ^{drd} of Eq. (2) may be neglected as a first approximation by choosing reasonable one-particle reference states, which in this work are chosen to be the Kohn-Sham eigenstates of density functional theory within the local density approximation(LDA) [30]. The first two terms of Eq. (2) can be calculated within the GW approximation [14–16] and have then the following form [29]:

$$\Sigma^d(1,2) = iG_0^d(1,2)W(1,2), \tag{3}$$

$$\Sigma^{rd}(1,2) = iG_0^r(1,2)W(1,2), \tag{4}$$

where G_0^r is the noninteracting Green's function for the electrons in the r space, and W is the screened Coulomb interaction. In correlated systems, the main low-energy structure of the self-energy is determined by Σ^d, while Σ^{rd} yields high-energy corrections [5].

While performing the downfolding procedure introduced in Ref. [29], the expression of the effective screened interaction among the electrons of the d subspace emerges naturally. Indeed, the screened interaction W is related to the bare Coulomb interaction V and the polarization function P according to

$$\begin{aligned} W(1,2) &= V(1,2) + \int d(34)V(1,3)P(3,4)W(4,2) \\ &= U(1,2) + \int d(34)U(1,3)P_d(3,4)W(4,2), \end{aligned} \tag{5}$$

where U is defined as

$$U(1,2) = V(1,2) + \int d(34)V(1,3)P_r(3,4)U(4,2). \tag{6}$$

In the above equations, P_d is the polarization function due to the electrons in the d subspace only, and $P_r = P - P_d$ is the polarization through r-r and r-d screening channels. The introduced quantity U is the partially screened Coulomb interaction and is related to the bare interaction V as in Eq. (6). Equation (5) suggests that this time- or frequency-dependent interaction U can be identified as the effective interaction in the low-energy model. This quantity may be calculated within the constrained random phase approximation (RPA) [31–33].

B. Low-energy dynamic model

From the previously described downfolding procedure [29], one can build an effective low-energy model for the d electrons. However, because of the frequency-dependent or retarded interaction U, one can only write this effective theory in the functional-integral formalism [34]. In one of the simplest models within this formalism, *only on-site* retarded interaction is considered and the effective action takes the following form [5]:

$$\begin{aligned} S_{\text{eff}} = \int d\tau\, d\tau' \Bigg[&\sum_{\mathbf{R}\mathbf{R}'nn'} c^\dagger_{\mathbf{R}n}(\tau)\left[\frac{\partial}{\partial\tau} - \mu + h_{nn'}(\mathbf{R}-\mathbf{R}')\right] \\ &\times c_{\mathbf{R}'n'}(\tau') + \frac{1}{2}\sum_{\mathbf{R}}\sum_{nn'mm'} U_{nn';mm'}(\tau-\tau') \\ &\times c^\dagger_{\mathbf{R}n}(\tau)c^\dagger_{\mathbf{R}m}(\tau')c_{\mathbf{R}m'}(\tau')c_{\mathbf{R}n'}(\tau)\Bigg], \end{aligned} \tag{7}$$

where $\mathbf{R}$ stands for the lattice site, n,m are the orbital indices, and μ is the chemical potential. The Grassman variables $c^{\dagger}_{\mathbf{R}n}$ and $c_{\mathbf{R}n}$ are associated to the creation and annihilation operators in the Wannier representation $\{w_{n\mathbf{R}}(\mathbf{r})\}$ of the low-energy model. In this expression, $h_{nn'}(\mathbf{R}-\mathbf{R}')$ are the matrix elements of the one-particle Kohn-Sham Hamiltonian within the LDA:

$$h_{nn'}(\mathbf{R}-\mathbf{R}') = \langle w_{n\mathbf{R}}|h|w_{n'\mathbf{R}'}\rangle \tag{8}$$

and $U_{nn';mm'}(\tau)$ is the on-site time-dependent interaction matrix:

$$U_{nn';mm'}(\tau) = \int d^3r\, d^3r'\, w^*_{n\mathbf{R}}(\mathbf{r}) w_{n'\mathbf{R}}(\mathbf{r}) U(\mathbf{r},\mathbf{r}',\tau) \times w^*_{m\mathbf{R}}(\mathbf{r}') w_{m'\mathbf{R}}(\mathbf{r}'). \tag{9}$$

While it includes all intra-atomic interaction, this model neglects long-range or intersite ($\mathbf{R} \neq \mathbf{R}'$) elements of the interaction.

C. Low-energy static model

One can build an effective model for the electrons in the d subspace which can take a Hamiltonian form by neglecting the frequency dependence of the interaction U. This is the commonly used Hubbard-like model with static on-site interactions:

$$H = \sum_{\mathbf{R},\mathbf{R}'nn'} h_{nn'}(\mathbf{R}-\mathbf{R}') c^{\dagger}_{\mathbf{R}n} c_{\mathbf{R}'n'} + \frac{1}{2}\sum_{\mathbf{R}} \sum_{n,n',m,m'} U_{nn';mm'} c^{\dagger}_{\mathbf{R}n} c^{\dagger}_{\mathbf{R}m} c_{\mathbf{R}m'} c_{\mathbf{R}n'}, \tag{10}$$

where $c^{\dagger}_{\mathbf{R}n}$ and $c_{\mathbf{R}n}$ are now the creation and annihilation operators. In this model, the on-site interaction matrix U corresponds to the *static* matrix elements of the screened interaction [5]

$$U_{nn';mm'} = U_{nn';mm'}(\omega = 0), \tag{11}$$

where the frequency-dependent interaction $U_{nn';mm'}(\omega)$ is obtained by the Fourier transformation of $U_{nn';mm'}(\tau)$ in Eq. (9). As discussed in Refs. [5,31], since the static effective interaction, which is given in Eq. (11), is one order of magnitude smaller than the bare Coulomb interaction, the energy scale of the self-energy calculated with this static interaction becomes much smaller than what is expected from first principles.

D. Self-energy within the GWA

Both the dynamic and static models can be treated within the GW approximation [14–16] but all quantities have to be expanded in terms of the Bloch functions $\phi_{\mathbf{k}n}$ constructed from the Wannier functions $w_{n\mathbf{R}}$ as

$$\phi_{\mathbf{k}n}(\mathbf{r}) = \frac{1}{\sqrt{N}} \sum_{\mathbf{R}} e^{i\mathbf{k}\cdot\mathbf{R}} w_{n\mathbf{R}}(\mathbf{r}), \tag{12}$$

where N is the number of unit cells in the calculation. The matrix elements of the effective interaction $U(\omega)$ with respect to the Bloch functions have a general form

$$U^{(\mathbf{k},\mathbf{k}')}_{nn';mm'}(\mathbf{q},\omega) = \int d^3r\, d^3r' [\phi^*_{\mathbf{k}n}(\mathbf{r})\phi_{\mathbf{k}+\mathbf{q}n'}(\mathbf{r})]^* U(\mathbf{r},\mathbf{r}';\omega) \times [\phi^*_{\mathbf{k}'m}(\mathbf{r}')\phi_{\mathbf{k}'+\mathbf{q}m'}(\mathbf{r}')], \tag{13}$$

and they become independent of $\mathbf{q}$, $\mathbf{k}$, and $\mathbf{k}'$, since in both the dynamic and static models, the effective interaction has only on-site components in the Wannier representation. The fully screened interaction matrix $W(\mathbf{q},\omega)$ is therefore calculated as

$$W(\mathbf{q},\omega) = [1 - U(\omega)P_d(\mathbf{q},\omega)]^{-1} U(\omega), \tag{14}$$

where P_d is the polarization function due to the d electrons:

$$P_{d\,nn';mm'}(\mathbf{q},\omega) = 2\sum_{\mathbf{k}\mu}^{occ}\sum_{\mathbf{k}'\nu}^{unocc} \delta_{\mathbf{k}',\mathbf{k}+\mathbf{q}} C^*_{n\mu}(\mathbf{k}) C_{n'\nu}(\mathbf{k}') C_{m\mu}(\mathbf{k}) C^*_{m'\nu}(\mathbf{k}') \times \left[\frac{1}{\omega - (\epsilon_{\mathbf{k}'\nu} - \epsilon_{\mathbf{k}\mu}) + i\eta} - \frac{1}{\omega + (\epsilon_{\mathbf{k}'\nu} - \epsilon_{\mathbf{k}\mu}) - i\eta}\right]. \tag{15}$$

Here η is a positive infinitesimal and the coefficients $C_{n\mu}(\mathbf{k})$ relate $\phi_{\mathbf{k}n}$ and the Kohn-Sham eigenstates $\psi_{\mathbf{k}\mu}$ which are obtained by diagonalizing the one-particle Hamiltonian $h_{nn'}(\mathbf{R})$, as

$$\psi_{\mathbf{k}\mu}(\mathbf{r}) = \sum_{n} C_{n\mu}(\mathbf{k}) \phi_{\mathbf{k}n}(\mathbf{r}). \tag{16}$$

One can see that in the on-site-only models, the momentum dependence of $W(\mathbf{q},\omega)$ comes only from P_d. In the case of the static model, $U(\omega)$ in Eq. (14) is replaced by its static value $U(\omega = 0)$.

For the model self-energy Σ^d, we first calculate the imaginary or anti-Hermitian part of it [35] by using the relation [36]

$$\langle\phi_{\mathbf{k}n}|\mathrm{Im}\,\Sigma^d(\omega)|\phi_{\mathbf{k}n'}\rangle = \sum_{\mathbf{q}\mu}\int d^3r\, d^3r' \phi^*_{\mathbf{k}n}(\mathbf{r})\psi_{\mathbf{k}-\mathbf{q}\mu}(\mathbf{r})\mathrm{Im}\,W(\mathbf{r},\mathbf{r}',\omega-\epsilon_{\mathbf{k}-\mathbf{q}\mu}) \times \psi^*_{\mathbf{k}-\mathbf{q}\mu}(\mathbf{r}')\phi_{\mathbf{k}n'}(\mathbf{r}') \times \begin{cases} +\theta(\omega-\epsilon_{\mathbf{k}-\mathbf{q}\mu})\theta(\epsilon_{\mathbf{k}-\mathbf{q}\mu}-\epsilon_F) & (\omega > \epsilon_F) \\ -\theta(\epsilon_{\mathbf{k}-\mathbf{q}\mu}-\omega)\theta(\epsilon_F-\epsilon_{\mathbf{k}-\mathbf{q}\mu}) & (\omega < \epsilon_F), \end{cases} \tag{17}$$

and then calculate the real or Hermitian part of the self-energy via the Kramers-Kronig transformation:

$$\langle\phi_{\mathbf{k}n}|\mathrm{Re}\,\Sigma^d(\omega)|\phi_{\mathbf{k}n'}\rangle = \langle\phi_{\mathbf{k}n}|\Sigma^d_x|\phi_{\mathbf{k}n'}\rangle - \frac{1}{\pi}\int_{-\infty}^{\infty} d\omega' \frac{\langle\phi_{\mathbf{k}n}|\mathrm{Im}\,\Sigma^d(\omega')|\phi_{\mathbf{k}n'}\rangle}{\omega-\omega'}\mathrm{sgn}(\omega'), \tag{18}$$

where Σ^d_x is the exchange part of the self-energy, and the Fermi level corresponds to $\omega = 0$. Since in our models U is local, the momentum dependence of the self-energy comes from W and P_d.

E. Self-energy within DMFT

DMFT is a quantitative method to handle electronic correlations In a nutshell, this approach treats the solid as

a set of single atoms embedded in an effective medium with which electronic transfers take place, this effective medium being self-consistently related to the rest of the solid. More precisely, the lattice problem is mapped onto a generalized Anderson impurity problem, whose solution yields a local (on-site) Green's function and a *local* self-energy that are identified as the on-site projection of the lattice solution [1–4].

In standard single-site DMFT, the atomic part of the impurity problem relies on an atomic multiorbital Hubbard model:

$$H = \sum_{\mathbf{R},\mathbf{R}'mm'\sigma} h_{mm'}(\mathbf{R}-\mathbf{R}')c^{\dagger}_{\mathbf{R}m\sigma}c_{\mathbf{R}'m'\sigma} + H_{\text{int}}, \quad (19)$$

where σ denotes now explicitly the spin. The interaction term $H_{\text{int}} = H_U + H_J$ is composed of a density-density term H_U:

$$H_U = \frac{1}{2}\sum_{\mathbf{R}}\sum_{m,m',\sigma} U^{\sigma\sigma}_{mm'} n_{\mathbf{R}m\sigma} n_{\mathbf{R}m'\sigma} + \frac{1}{2}\sum_{\mathbf{R}}\sum_{m,m'} U^{\uparrow\downarrow}_{mm'}(n_{\mathbf{R}m\uparrow}n_{\mathbf{R}m'\downarrow} + n_{\mathbf{R}m\downarrow}n_{\mathbf{R}m'\uparrow}), \quad (20)$$

where $n_{\mathbf{R}m\sigma} = c^{\dagger}_{\mathbf{R}m\sigma}c_{\mathbf{R}m\sigma}$, and a nondensity-density term H_J which contains the so-called "spin-flip" and "pair-hopping" terms:

$$H_J = -\frac{1}{2}\sum_{\mathbf{R}}\sum_{m,m'} J_{mm'}(c^{\dagger}_{\mathbf{R}m\uparrow}c_{\mathbf{R}m\downarrow}c^{\dagger}_{\mathbf{R}m'\downarrow}c_{\mathbf{R}m'\uparrow} + \text{H.c.}) - \frac{1}{2}\sum_{\mathbf{R}}\sum_{m,m'} J_{mm'}(c^{\dagger}_{\mathbf{R}m\uparrow}c^{\dagger}_{\mathbf{R}m\downarrow}c_{\mathbf{R}m'\uparrow}c_{\mathbf{R}m'\downarrow} + \text{H.c.}). \quad (21)$$

The introduced interaction parameters are related to the static on-site effective interaction U in Eq. (11) by the following relations [37]:

$$\begin{aligned} U^{\sigma\bar{\sigma}}_{mm'} &= U_{mm;m'm'}, \\ J_{mm'} &= U_{mm';m'm}, \quad m \neq m', \\ U^{\sigma\sigma}_{mm'} &= U_{mm;m'm'} - U_{mm';m'm}, \quad m \neq m'. \end{aligned} \quad (22)$$

By treating the static model within DMFT, the effective self-energy Σ^d within DMFT is "local" in Wannier representation; namely, when expanded in terms of the Wannier functions $w_{n\mathbf{R}}(\mathbf{r})$, the self-energy has only site-diagonal elements [38]:

$$\langle w_{n\mathbf{R}}|\Sigma^d(\omega)|w_{n'\mathbf{R}'}\rangle = \delta_{\mathbf{R}\mathbf{R}'}\Sigma^d_{nn'}(\omega). \quad (23)$$

In the reciprocal space, this implies that Σ^d is $\mathbf{k}$ independent:

$$\langle \phi_{\mathbf{k}n}|\Sigma^d(\omega)|\phi_{\mathbf{k}n'}\rangle = \Sigma^d_{nn'}(\omega). \quad (24)$$

Equation (24) can be verified by substituting $\phi_{\mathbf{k}n}$ in Eq. (12) into Eq. (24) and using Eq. (23).

Recently, methods have also been developed to include dynamical screening and solve the dynamic model as defined in Eq. (7) within DMFT [9–11]. First applications to the dynamic model show a substantial band renormalization which is not accounted for in the static model [6–8]. However, the treatment of the dynamic model within DMFT is beyond the scope of this work.

F. Aim/Principle of the study

The main purpose of this work is to compare the *ab initio* self-energy within the GWA, with the effective self-energy Σ^d in Eq. (2), calculated in the model GW calculation and in DMFT. Within the GWA, we can also compute the d contribution of the self-energy $\Sigma^d = G^d_0 W$ from first principles without any ambiguity. In this work, we focus on spin-unpolarized Fe and $SrVO_3$ as test materials. The d space in the model consists of the five d orbitals for Fe and does not include the $4s$ band, whereas it contains only the three t_{2g} orbitals for $SrVO_3$.

In the first part, the *ab initio* GW self-energy is directly compared with the self-energy within the static and dynamic models, whose parameters, including the effective interaction $U(\omega)$, are calculated from first principles. In the second part, we discuss the correlation effects for these systems by comparing the self-energy in the static model calculated within the GWA and DMFT.

III. COMPARISON OF DOWNFOLDED SELF-ENERGY WITHIN THE GWA

A. Computational details

In this work, the LDA and *ab initio* GW calculations are performed with the full-potential linearized augmented plane-wave DFT code FLEUR [39] and the GW code SPEX [40]. We employ the Perdew-Zunger parametrization [41] of the LDA exchange-correlation functional. The lattice constants used in this work are $a = 5.42$ bohr for bcc Fe and $a = 7.26$ bohr for cubic $SrVO_3$. In both systems $8 \times 8 \times 8$ $\mathbf{k}$-point sampling is used. To compute the polarization and Green's function in the GWA, around 50 and 380 unoccupied bands are used for Fe and $SrVO_3$, respectively. As basis functions $w_{n\mathbf{R}}$ for the models, we use the maximally localized Wannier functions [42–44]. We use a recently proposed symmetry-constrained routine [45] to construct symmetry-adapted Wannier functions using a customized version of the WANNIER90 library [46]. The frequency-dependent screened interactions are calculated using the constrained RPA [31–33] implemented in the SPEX code [40].

In the effective models, the self-energy correction induces a large change in the chemical potential, due to the double counting of the exchange-correlation effects. To fix this change, in the GW calculations we use Hedin's approach [14,47], which amounts to adding the following term to the effective Hamiltonian:

$$H' = -\Delta\sum_{\mathbf{R}n} c^{\dagger}_{\mathbf{R}n}c_{\mathbf{R}n}, \quad (25)$$

where the shift Δ is evaluated as

$$\Delta = \text{Re}\langle\psi_{\mathbf{k}'\mu'}|\Sigma^0(\epsilon_{\mathbf{k}'\mu'})|\psi_{\mathbf{k}'\mu'}\rangle. \quad (26)$$

Here the prime ($'$) denotes the state at or closest to the Fermi energy, and Σ^0 is the GW self-energy calculated in the model without this shift.

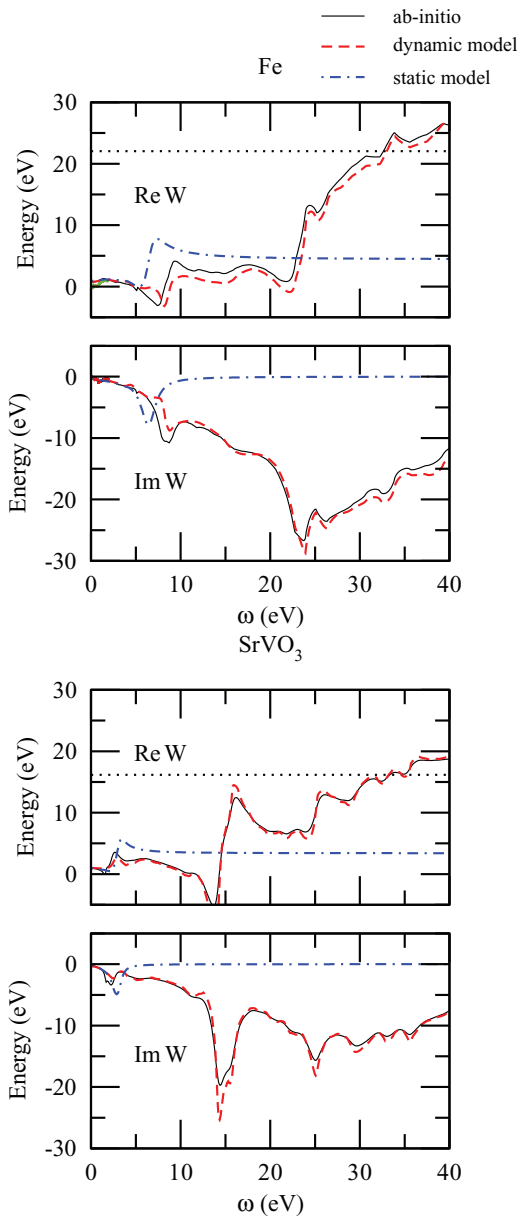

FIG. 1. (Color online) On-site average diagonal matrix elements of the screened interaction $W(\omega)$ for Fe and $SrVO_3$. The dotted lines show the values of the bare Coulomb interaction.

B. Results and discussion

1. *Fully screened interaction W and self-energy*

We first discuss the fully screened interaction W [Eq. (5)], which is related to the GW self-energy through Eq. (17). In Fig. 1 we plot the frequency dependence of the average on-site value of the fully screened interaction defined as

$$\bar{W}(\omega) = \frac{1}{N_d}\sum_{n\in d}\langle w_{n\mathbf{R}}w_{n\mathbf{R}}|W(\omega)|w_{n\mathbf{R}}w_{n\mathbf{R}}\rangle = \frac{1}{N_d}\sum_{n\in d}\int d^3r\, d^3r' w^*_{n\mathbf{R}}(\mathbf{r})w_{n\mathbf{R}}(\mathbf{r})W(\mathbf{r},\mathbf{r}',\omega) \times w^*_{n\mathbf{R}}(\mathbf{r}')w_{n\mathbf{R}}(\mathbf{r}'), \quad (27)$$

where N_d is the number of orbitals in the d subspace (i.e., $N_d = 5$ for Fe and $N_d = 3$ for $SrVO_3$), for the *ab initio* and model calculations. The high-energy structure of $W(\omega)$ is mainly determined by the plasmonlike peaks at around 25 eV for Fe and 15 eV for $SrVO_3$, and above these energies the screening is less effective and the screened interaction approaches the bare (unscreened) Coulomb interaction. The dynamic model well reproduces the high-energy part of the on-site fully screened interaction of the *ab initio* calculation, while a deviation is seen in the low-energy part of Fe at around 5–10 eV. The structure seen in this region originates from particle-hole polarizations between the d states of Fe modulated by the interaction term, therefore this difference may indicate that for Fe there is a large contribution of the intersite polarization process to the screening. This deviation can also be due to the entanglement between $3d$ and $4s$ bands in the *ab initio* calculation, which is removed in our model calculations. The static model gives a structure only in the low-energy region through particle-hole excitations within the bandwidth of the correlated bands, and for frequencies above ∼10 eV Re $W(\omega)$ in the static model quickly goes to $U(\omega = 0)$, which in our calculations is 4.4 and 3.4 eV for Fe and $SrVO_3$, respectively. The static ($\omega = 0$) values of these interactions are well explained by these models; they are 0.7 and 0.9 eV for Fe and $SrVO_3$, respectively.

We now investigate the frequency and momentum dependence of the *ab initio* GW self-energy for localized d states, which takes into account the full interaction. In Figs. 2–4, we plot the momentum-dependent *ab initio* GW self-energy projected onto d orbitals $\langle\phi_{\mathbf{k}n}|\Sigma(\omega)|\phi_{\mathbf{k}n}\rangle$ ($n \in t_{2g}, e_g$), where $\phi_{\mathbf{k}n}$ is given in Eq. (12), for Fe and $SrVO_3$ at some high-symmetry points. In the figures we also plot two additional quantities: (i) the self-energy correction to the Kohn-Sham Hamiltonian $\langle\phi_{\mathbf{k}n}|\Sigma - V_{xc}|\phi_{\mathbf{k}n}\rangle$, which is more relevant for usual GW calculations, especially for evaluating the quasiparticle band structure, and (ii) the d contribution to the self-energy $\Sigma^d = G^d_0 W$, which corresponds to the self-energy calculated in the effective models.

In both systems, the real part of the full self-energy, shown in the top-left panels of the figures, has a large $\mathbf{k}$ dependence, and at some $\mathbf{k}$ points such as the N point in the case of Fe t_{2g}, the self-energy has orbital dependence as well. By comparing the full self-energy with its d contribution $G^d_0 W$ (top-right panels), which shows a weaker $\mathbf{k}$ dependence, one can see that the main contribution of this $\mathbf{k}$ dependence comes from the exchange and correlation between electrons in the d and r spaces $\Sigma^{rd} = G^r_0 W$. Since, in the Wannier representation, the $\mathbf{k}$ dependence of the self-energy comes from its intersite components $\langle w_{n\mathbf{R}}|\Sigma|w_{n'\mathbf{R}'}\rangle$ ($\mathbf{R} \neq \mathbf{R}'$), this implies that Σ^{rd} has large intersite components. On the other hand, the d components of the self-energy $\Sigma^d = G^d_0 W$ exhibit a weaker $\mathbf{k}$ dependence and therefore smaller intersite components than those of Σ^{rd}. In the Wannier representation, the intersite components of Σ^d are expressed as

$$\langle w_{n\mathbf{R}}|\Sigma^d|w_{n'\mathbf{R}'}\rangle = \sum_{\mathbf{R}_1\mathbf{R}_2}\sum_{mm'} G^d_{\mathbf{R}_1 m;\mathbf{R}_2 m'} \times\langle w_{n\mathbf{R}}w_{m\mathbf{R}_1}|W|w_{m'\mathbf{R}_2}w_{n'\mathbf{R}'}\rangle, \quad (28)$$

where $G^d_{\mathbf{R}_1 m;\mathbf{R}_2 m'}$ is the matrix elements of G^d_0 with respect to the Wannier orbitals, which shows that this small but nonzero

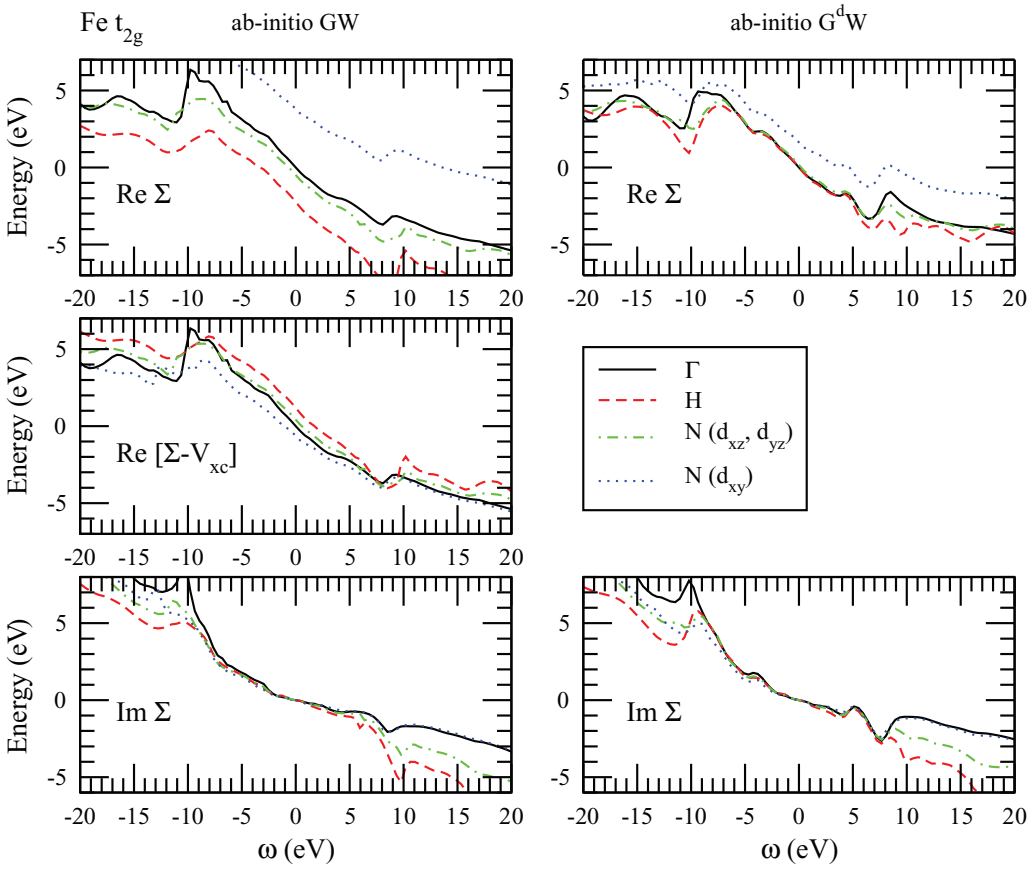

FIG. 2. (Color online) *Ab initio GW* self-energy and self-energy correction to the LDA Kohn-Sham Hamiltonian ($\Sigma - V_{xc}$) for the t_{2g} orbitals of Fe at $\mathbf{k} = \Gamma(0,0,0)$, $H(\frac{2\pi}{a},0,0)$, and $N(\frac{\pi}{a},\frac{\pi}{a},0)$. Right panels show the d contribution to the self-energy ($\Sigma^d = G_0^d W$). The real parts of these quantities are measured relative to the corresponding values for $\mathbf{k} = \Gamma$ at $\omega = 0$.

k dependence of Σ^d can be traced back to the intersite matrix elements of the screened interaction W.

By subtracting the exchange-correlation potential V_{xc} from the full self-energy, as shown in the middle panels of the figures, the large **k** dependence of the full self-energy is largely canceled, which indicates that the contribution arising from the r space may be well described by the static exchange-correlation potential V_{xc}; however, the cancellation is not perfect and the self-energy correction $\Sigma - V_{xc}$ and the d contribution of the self-energy $G_0^d W$ have a different **k** dependence. The difference between these two with respect to **k** points is comparable to the bandwidth of the d states, which can affect the quasiparticle energies. This result shows that solving the effective models including the d electrons only is not enough to reproduce the quasiparticle band structure obtained from the *ab initio GW* results, without a proper (nontrivial) momentum-dependent double-counting correction term which effectively includes both the r-d correlations and the exchange-correlation term V_{xc}. Although the present calculations and discussions are based on the GWA, the true effective self-energy is expected to have similar **k** dependence if long-range exchange and correlation is taken into account.

In Figs. 5 and 6, we plot the self-energies calculated in the static and dynamic models at some **k** points. To make a comparison between *ab initio* and model calculations, in the figures we also plot the on-site component of the self-energy given by

$$\Sigma_{nn}^{\text{local}}(\omega) = \langle w_{n\mathbf{R}}|\Sigma(\omega)|w_{n\mathbf{R}}\rangle = \frac{1}{N}\sum_{\mathbf{k}}\langle\phi_{\mathbf{k}n}|\Sigma(\omega)|\phi_{\mathbf{k}n}\rangle \quad (29)$$

obtained from the *ab initio* $G_0^d W$ calculations. In contrast to the full *ab initio GW* results shown in Figs. 2–4, we find that in these models, which include only on-site interactions, the self-energies show very weak **k** dependence, indicating in these models the self-energy becomes almost local (site diagonal). This small **k** dependence, which is only visible at around -8 eV for Fe and -3 eV for $SrVO_3$ in the static model results, arises from the intersite polarization P_d through the **k**-dependent particle-hole excitations, since the interaction has on-site components only. A comparison between these model self-energies and the *ab initio*, **k**-dependent self-energy in Figs. 2–4 indicates that the long-range component of the effective interaction has a larger impact on the momentum dependence of the self-energy than the momentum dependence of the polarization. As can be seen from the figures, the local (on-site) part of the self-energy within the $G_0^d W$ and the dynamic model self-energy are found to be very close, as this model takes into account the high-energy contribution to the self-energy, namely, the r-d polarization and plasmon excitations through the frequency dependence of $U(\omega)$. This is

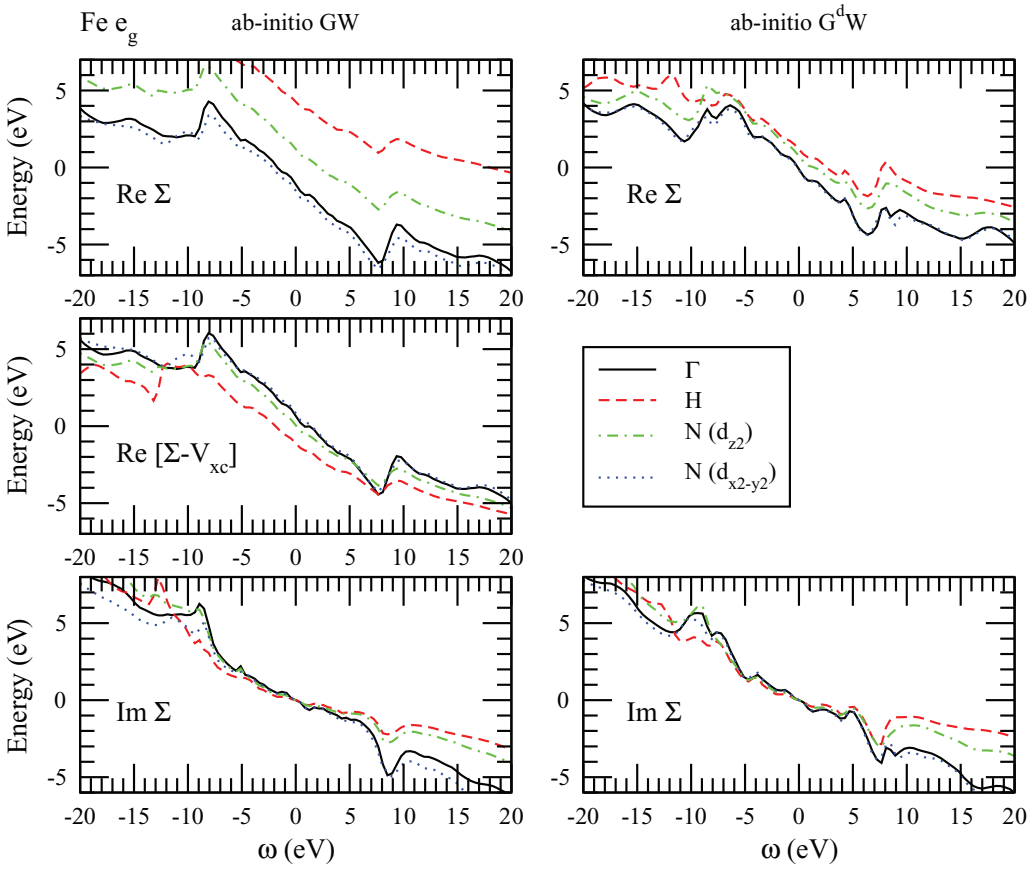

FIG. 3. (Color online) Same as Fig. 2 but for the e_g orbitals of Fe. The real parts of these quantities are measured relative to the corresponding values for the t_{2g} orbitals (Fig. 2) for $\mathbf{k} = \Gamma$ at $\omega = 0$.

also consistent with the fact that the dynamic model reproduces overall structures of the on-site part of the fully screened interaction as shown in Fig. 1. The static model also reproduces the low-energy structure of the *ab initio* results for Im $\Sigma(\omega)$, as the low-energy structure of the imaginary part of the self-energy, which is determined by the low-energy structure of Im $W(\omega)$, is mainly determined by the excitations of the electrons within the d subspace, as seen in Fig. 1. However, Im $\Sigma(\omega)$ at high energy is essentially zero due to the missing high-energy component of the screened interaction. Since Im $\Sigma(\omega)$ of the static model has no high-energy component, the real part of the self-energy is not well reproduced as can be understood from the expression for Re $\Sigma(\omega)$ in Eq. (18). The real part of the self-energy in the static model also has a smaller slope compared to the *ab initio* $G_0^d W$ one, which leads to a smaller renormalization of quasiparticles and this also affects the bandwidth of d states, as shown in the next section. A similar conclusion was reached in Ref. [48]. This difference can also be important for discussing possible satellite structures, as discussed in Ref. [5] in the case of Ni; in the static GW result of Fe, a strong variation on Re $\Sigma(\omega)$ is seen at around -10 eV, but this seems an artifact of using a static U.

2. *Quasiparticle band structure*

We now compare the quasiparticle band structures of Fe and $SrVO_3$ calculated from the model and *ab initio* self-energies. We use a Wannier-interpolation technique [43,49] to calculate the quasiparticle energies for d states at arbitrary $\mathbf{k}$ points. In a previous work [13], it was found that ignoring the $\mathbf{k}$ dependence of the *full* self-energy [i.e., $\Sigma^{\rm eff}$ in Eq. (2)] causes band narrowing of the correlated bands. We find that this tendency also holds for the model results as shown in Fig. 7, albeit the momentum dependence is weak. The static model also yields a wider bandwidth than that of the dynamic model, resulting in fortuitously better agreement with the *ab initio* GW results. The quasiparticle renormalization is therefore larger in the dynamic than in the static model. This larger renormalization due to the dynamic screening is consistent with recent DMFT calculations with frequency-dependent interactions by Casula *et al.* and Werner *et al.* [6,7]. As seen in Figs. 5 and 6, including the dynamic screening transfers large weights from the quasiparticle peaks to high-energy regions, resulting in a larger renormalization and hence a larger band narrowing. The effects of frequency-dependent U and $\mathbf{k}$ dependence of the self-energy tend to cancel each other so that the static model results are closer to the *ab initio* GW results. To analyze this effect more quantitatively, in Table I we tabulate the bandwidth reduction of Fe and $SrVO_3$ from the LDA bandwidth. In the usual GWA, the bandwidth reduction is around 0.8–0.9 for these systems, while if we use the local (but *full*) self-energy, as done in Ref. [13], we get a larger reduction of around 0.6. The results of the dynamical model show a similar reduction, as the self-energy calculated in this

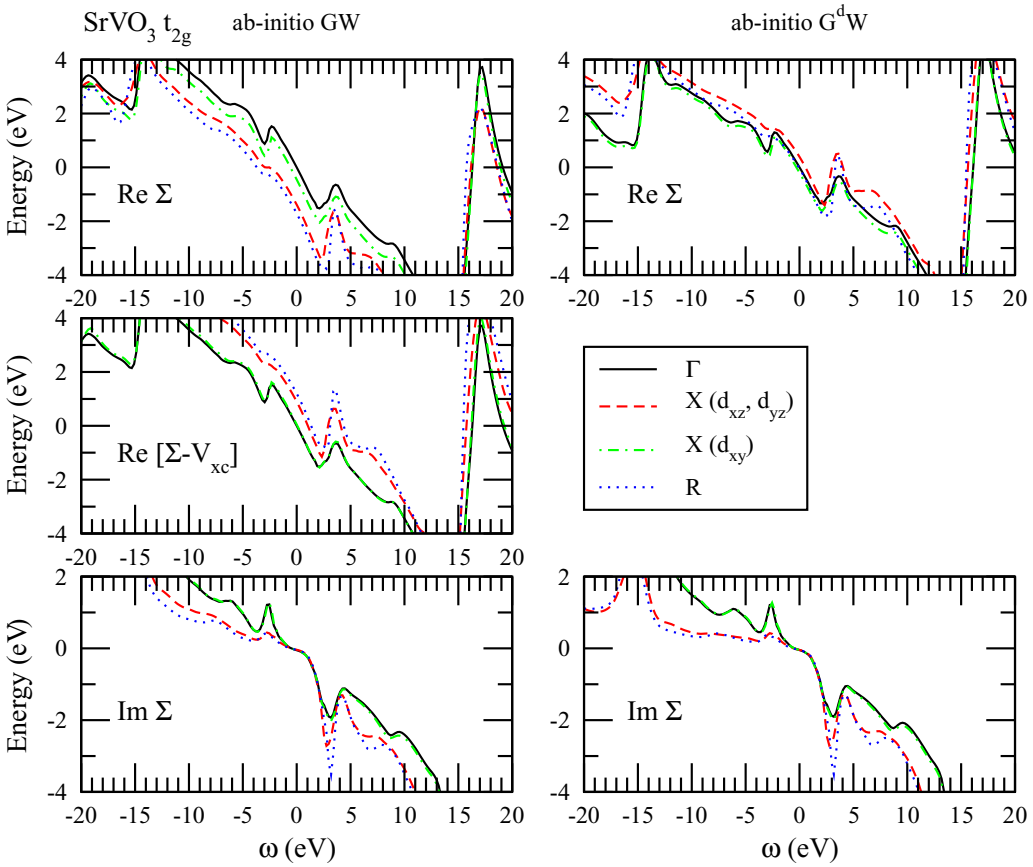

FIG. 4. (Color online) *Ab initio GW* self-energy and self-energy correction to the LDA Kohn-Sham Hamiltonian ($\Sigma - V_{xc}$) for the t_{2g} orbitals of $SrVO_3$ at $\mathbf{k} = \Gamma(0,0,0)$, $X(0,0,\frac{\pi}{a})$, and $R(\frac{\pi}{a},\frac{\pi}{a},\frac{\pi}{a})$. Right panels show the d contribution to the self-energy ($\Sigma^d = G_0^d W$). The real parts of these quantities are measured relative to the corresponding values for $\mathbf{k} = \Gamma$ at $\omega = 0$.

model is very close to that of the localized GW self-energy, whereas the static model gives a smaller reduction of ∼0.7. In summary, for these systems the bandwidth within the GWA is reduced by approximately 20% (13%) and 34% (28%) for Fe ($SrVO_3$) in the static model and the dynamic model, respectively, compared to the *ab initio GW* calculation. This difference in the bandwidth reduction between the full and model calculations comes from the **k** dependence of the self-energy which is not well accounted for in the usual model calculations. The deviation is larger in Fe compared to $SrVO_3$, meaning that the nonlocal interaction is more important in Fe. This result can be due to an itinerant character of the d electrons in this system.

IV. COMPARISON BETWEEN THE GWA AND DMFT

A. Computational details for DMFT

In this work, the DMFT calculation is performed by using the TRIQS libraries package [50]. For practical reasons, the effective model is built out of the LDA calculations performed with the electronic structure code WIEN2K [51], using the Wannier projectors calculated with the interface WIEN2TRIQS [52]. The basis functions of the model $w_{n\mathbf{R}}$ are thus not constructed following the prescription of maximal localization, but by promoting atomic orbitals to Wannier functions thanks to a truncated expansion over Bloch functions followed by an orthonormalization procedure. Whereas these two approaches give similar results in the case of $SrVO_3$ because the t_{2g} bands are well separated from others, some small discrepancies may appear in the definition of d orbitals of paramagnetic Fe because of their entanglement with the 4s band [53].

The quantum impurity problem has been solved by the numerically exact continuous-time quantum Monte Carlo (CTQMC) method in the strong-coupling formulation [54]. We perform calculations at room temperature ($\beta = 1/k_B T = 40\ \text{eV}^{-1}$) and use typically around 16×10^6 Monte Carlo sweeps and 35 (44) **k** points in the irreducible Brillouin zone for $SrVO_3$ (Fe). To take advantage of a maximal amount of conserved quantum numbers, we keep only the density-density terms defined in Eq. (20) for the local interaction H_{int} [55].

The reduced interaction matrices $U^{\sigma\bar{\sigma}}_{mm'}$ and $U^{\sigma\sigma}_{mm'}$ in Eq. (20) can be linked to the local effective Coulomb interaction $U(\omega = 0)$ of the previous GW calculations using the relations in Eq. (22). However, we rather parametrize the local interaction with a Hubbard term $\mathcal{U}$ and a Hund's coupling $\mathcal{J}$ so that the used double-counting corrections may be well defined. These parameters are set in order to get the best agreement between the calculated reduced interaction matrices and the matrix elements of $U(\omega = 0)$ from our previous GW calculations. For the three t_{2g} orbitals or $SrVO_3$, we find $\mathcal{U} = 3.40$ eV and $\mathcal{J} = 0.46$ eV directly from a Hubbard-Kanamori parametrization of the local interaction

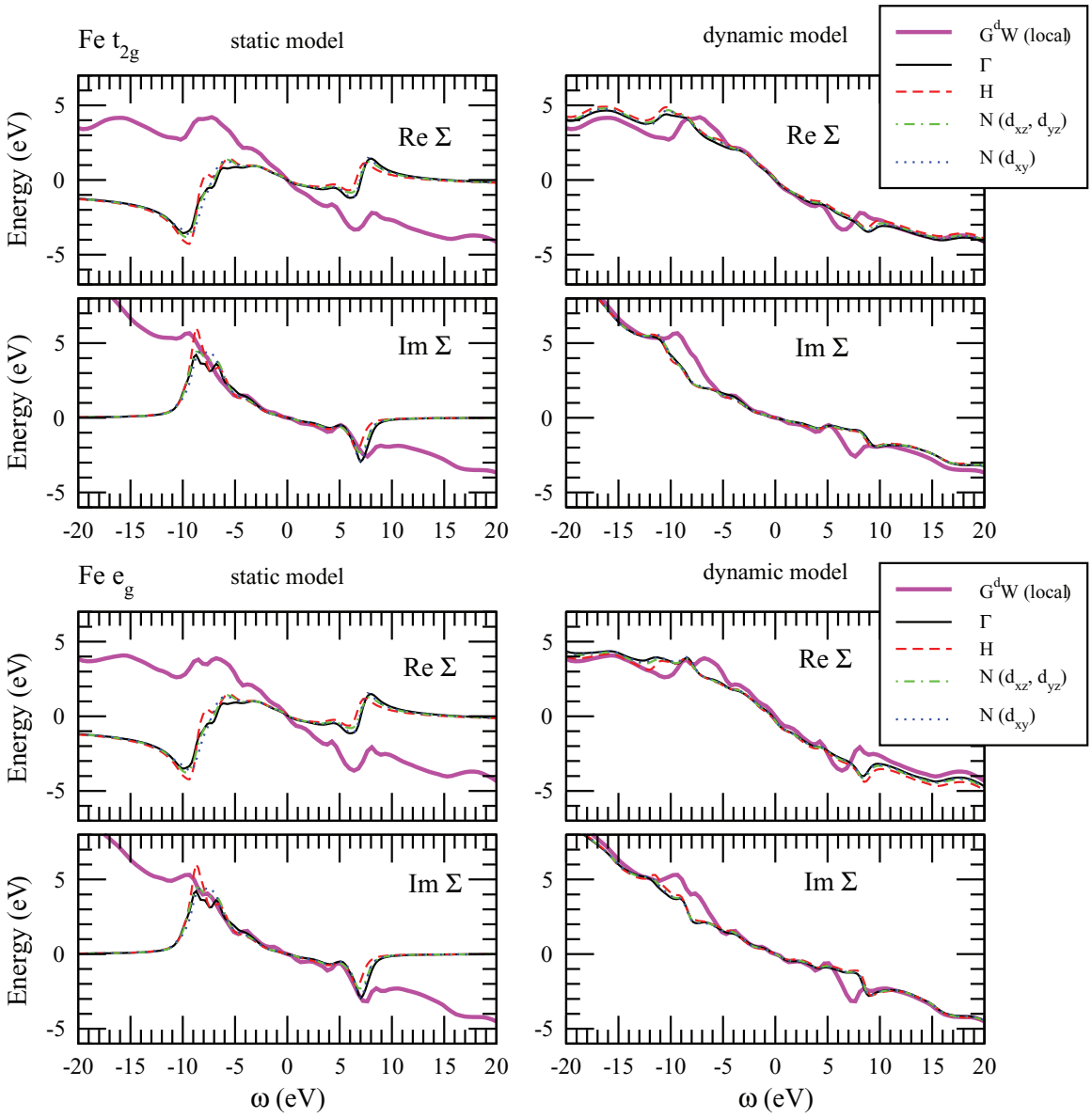

FIG. 5. (Color online) *GW* self-energy within the static and dynamic models at some high-symmetry **k**-points for t_{2g} and e_g orbitals of Fe. Thick lines show the local part of the *d*-contribution of the *ab initio* self-energies. The real parts of these quantities are measured relative to the corresponding values of the t_{2g} orbitals for $\mathbf{k} = \Gamma$ at $\omega = 0$.

$U(\omega = 0)$. For the five d orbitals of Fe, we parametrize the local interaction $U(\omega = 0)$ with Slater integrals F^0, F^2, and F^4 while assuming the ratio $F^2/F^4 = 0.63$. This leads to the values $\mathcal{U} = 3.37$ eV and $\mathcal{J} = 0.97$ eV thanks to the following relations [37,56,57]:

$$\mathcal{U} = F^0 \quad \text{and} \quad \mathcal{J} = (F^2 + F^4)/14. \tag{30}$$

In the Appendix, we list the obtained values of the reduced interaction matrices $U^{\sigma\bar{\sigma}}_{mm'}$ and $U^{\sigma\sigma}_{mm'}$ used in our model for both compounds.

To remove the part of correlations that are already taken into account in the LDA, we use the double-counting correction referred to as the fully localized limit [58] for $SrVO_3$:

$$\Sigma^{\sigma,dc\ FFL}_{m,m'} = \left[\mathcal{U}\left(N_c - \frac{1}{2}\right) - \mathcal{J}\left(N^\sigma_c - \frac{1}{2}\right)\right]\delta_{mm'}, \tag{31}$$

where N^σ_c is the spin-resolved occupancy of the correlated orbitals and $N_c = N^\uparrow_c + N^\downarrow_c$. For Fe, we use the around mean-field correction [59]:

$$\Sigma^{\sigma,dc\ AMF}_{m,m'} = \left[\mathcal{U}\left(N_c - \frac{\langle n_c\rangle}{2}\right) - \mathcal{J}\left(N^\sigma_c - \langle n^\sigma_c\rangle\right)\right]\delta_{mm'}, \tag{32}$$

where $\langle n^\sigma_c\rangle$ is the mean value of the spin-resolved occupancy of the orbitals and $\langle n_c\rangle = \langle n^\uparrow_c\rangle + \langle n^\downarrow_c\rangle$.

Finally, since the CTQMC solver computes the Green's function on the imaginary-time axis, an analytic continuation is needed in order to obtain results on the real-frequency axis. This continuation of the impurity self-energy is performed with an implementation of the maximum entropy method as the mean-field version of the stochastic analytic continuation

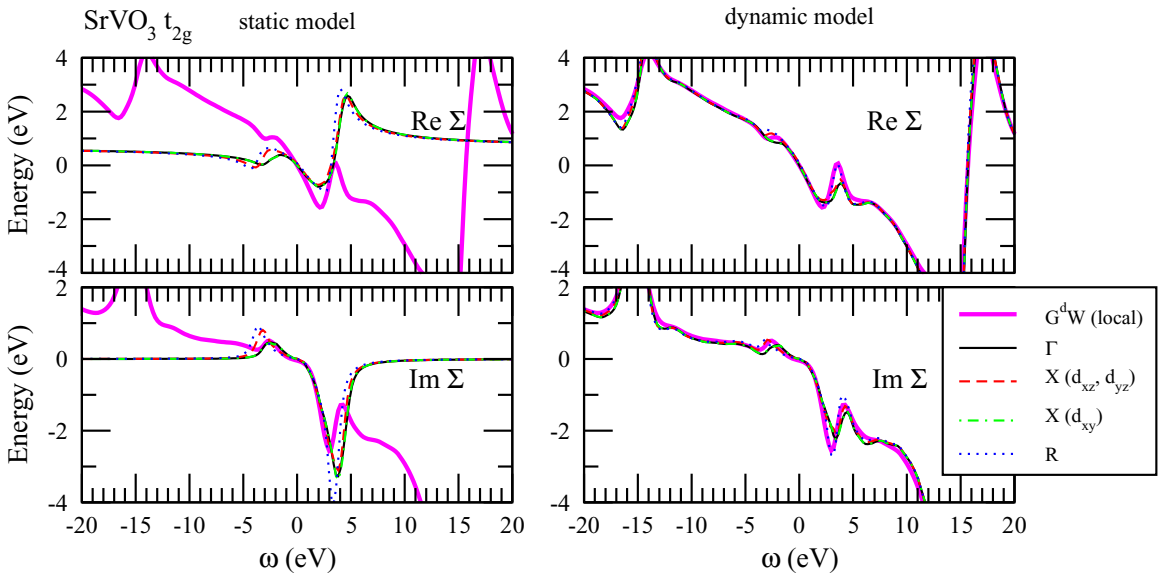

FIG. 6. (Color online) GW self-energy calculated in the static and dynamic models at some high-symmetry $\mathbf{k}$ points for t_{2g} orbitals of $SrVO_3$. Thick lines show the local part of the d contribution of the *ab initio* self-energies. The real parts of these quantities are measured relative to the corresponding values for $\mathbf{k} = \Gamma$ at $\omega = 0$.

method [60] and yields real and imaginary parts of the retarded self-energy.

B. Self-energy in the GWA and DMFT

We now compare the frequency dependence of the self-energy for the static model of paramagnetic Fe and $SrVO_3$, calculated within the GWA and LDA + DMFT. In Figs. 8 and 9, we plot the physical (retarded) self-energy, which is more natural in DMFT calculations than the time-ordered one commonly used in the GWA. A major difference between the GW and DMFT results in Fig. 8 is the position of the peaks in Im $\Sigma(\omega)$; the DMFT result shows a peak at around -3 eV for both orbitals and also a weaker peak at around $+3$ eV for e_g, while in the GW result for the static model, the peaks are located at higher energy, and in the dynamic model the peaks are further pushed away to a higher region due to the high-energy structure of the frequency-dependent interaction. This appears to be a general problem with the GWA which tends to overestimate satellite binding energies. Indeed, similarly, in Fig. 9, the peaks of Im $\Sigma(\omega)$ in DMFT are located closer to $\omega = 0$ than in the GWA for $SrVO_3$; in the GW results, both static and dynamic models show two peaks at around ± 3 eV, which originate from the peak at ≈ 2 eV in Im $W(\omega)$ (Fig. 1) and are traced back to d-d particle-hole excitations, as also discussed by Gatti *et al.* [28]. As shown in previous DMFT works [8,24,26], the peaks in the DMFT self-energy produce some satellite features in the spectral function at $\approx \pm 2$ eV known as Hubbard bands, while in the GWA within the static model, these peaks being higher in energy, the corresponding features are also located too high compared to experiment [61].

TABLE I. Reduction of the bandwidth D from the LDA result $\frac{D_{GW}}{D_{\mathrm{LDA}}}$ averaged over all $\mathbf{k}$ points in various GW calculations. The bandwidth at each $\mathbf{k}$ point is calculated as $\max(\{E_{\mathbf{k}\mu}\}, E_F) - \min(\{E_{\mathbf{k}\mu}\}, E_F)$, where $E_{\mathbf{k}\mu}$ and E_F are the quasiparticle energies and the Fermi energy, respectively. The label GW (local) refers to the result using the local GW self-energy as done in Ref. [13].

$\frac{D_{GW}}{D_{\mathrm{LDA}}}$	GW	GW (local)	Dynamic model	Static model
Fe	0.92	0.67	0.60	0.74
$SrVO_3$	0.82	0.55	0.59	0.71

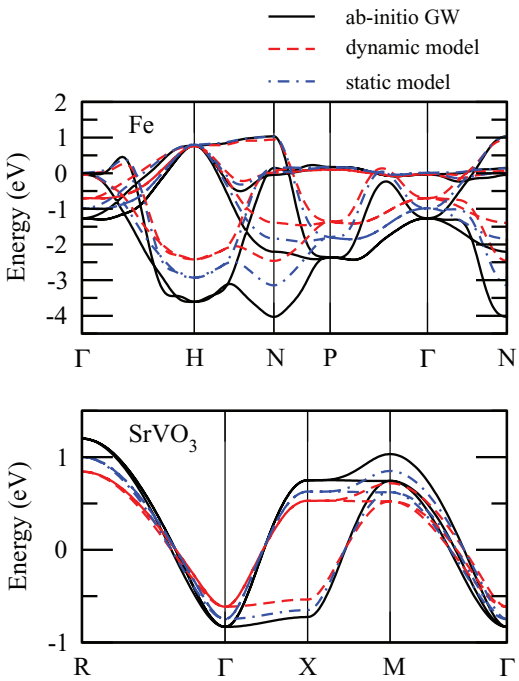

FIG. 7. (Color online) Quasiparticle band structure of Fe and $SrVO_3$.

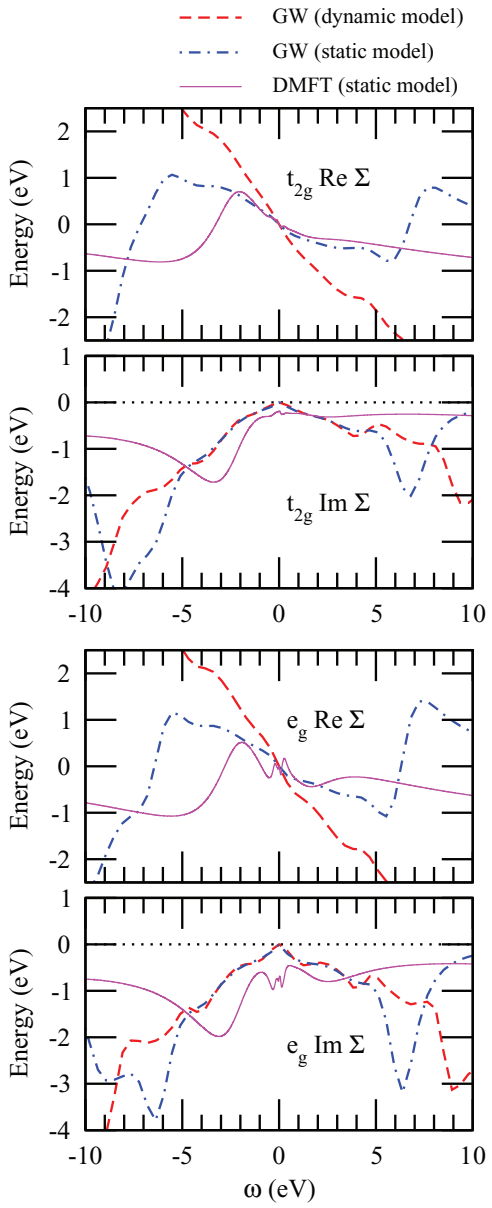

FIG. 8. (Color online) Self-energy of Fe calculated within the model GWA and DMFT. To make comparison easier the data in the upper figure are shifted so that $\mathrm{Re}\,\Sigma(\omega=0)=0$. Note that the presented self-energies here are the retarded ones $\Sigma^{\mathrm{R}}(\omega)$, which are related to the time-ordered self-energies as $\mathrm{Re}\,\Sigma^{\mathrm{R}}(\omega)=\mathrm{Re}\,\Sigma(\omega)$ and $\mathrm{Im}\,\Sigma^{\mathrm{R}}(\omega)=\mathrm{Im}\,\Sigma(\omega)\mathrm{sgn}(\omega)$.

Another noticeable difference between the GW and the DMFT results for Fe is the nonzero $\mathrm{Im}\,\Sigma(\omega)$ at $\omega=0$ in the DMFT results, which is also reported in the previous LDA + DMFT work by Katanin *et al.* [21]. This non-Fermi-liquid behavior is stronger for e_g orbitals, indicating that in this system these orbitals are more correlated than t_{2g} orbitals, and this behavior is not captured in the GWA. Interestingly, for the t_{2g} orbitals both the DMFT and GW results with static U show a similar slope of $\mathrm{Re}\,\Sigma(\omega)$ near $\omega=0$, which may be another indication of the itinerant character of the t_{2g} orbitals. As discussed in the previous section, including the frequency dependence yields a larger renormalization effect, as seen

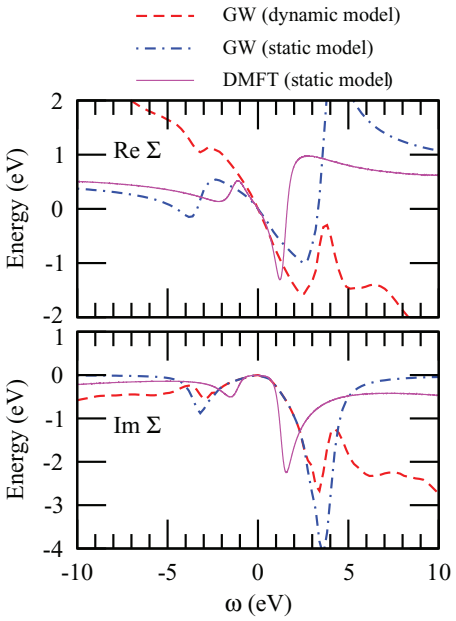

FIG. 9. (Color online) Retarded self-energy of $SrVO_3$ calculated within the model GWA and DMFT. To make comparison easier the data in the upper figure are shifted so that $\mathrm{Re}\,\Sigma(\omega=0)=0$.

from the slope of $\mathrm{Re}\,\Sigma(\omega)$ in Fig. 8. Studying the effects of dynamical screening on this non-Fermi-liquid behavior of this system in DMFT would be an interesting subject, which will be investigated in our future work.

Due to the low-energy peaks in $\mathrm{Im}\,\Sigma(\omega)$ within DMFT, the real part of the self-energy is expected to give a larger slope of $\mathrm{Re}\,\Sigma(\omega)$ near $\omega=0$ than the static GW result. Since the DMFT self-energy does not have $\mathbf{k}$ dependence, the renormalized factor calculated from this slope as $Z=[1-\frac{\partial\,\mathrm{Re}\,\Sigma(\omega)}{\partial\omega}|_{\omega=0}]^{-1}$ yields directly the quasiparticle band narrowing. On the contrary, since the peaks in $\mathrm{Im}\,\Sigma(\omega)$ are located higher in energy in the GW results, the GW result yields a weaker renormalization effect. Indeed, for $SrVO_3$, the slope of $\mathrm{Re}\,\Sigma(\omega)$ gives a renormalization of $\sim$0.5 for the t_{2g} bands, as observed in other DMFT calculations [24]. This is comparable to the dynamic result, while the static GW result is around 0.7. For Fe, we cannot draw a similar and clear conclusion: While the slope of $\mathrm{Re}\,\Sigma(\omega)$ near $\omega=0$ for the t_{2g} is similar in the DMFT and GW results with static U, the non-Fermi-liquid behavior of e_g prevents one from clearly evaluating the slope close to $\omega=0$.

The main difference between GW and DMFT can be explained by neglecting higher-order terms of the self-energy expansion with respect to W in the GWA. It is known that including vertex correction via the cumulant expansion improves the peak position of plasmon satellites [62,63]. As seen in Fig. 1, the strongly correlated materials like $SrVO_3$ show a low-energy peak in $\mathrm{Im}\,W(\omega)$ due to particle-hole excitations between localized electrons [28,64–66], and the positions of these so-called "subplasmon" peaks may also be corrected by the cumulant expansion. Indeed, recently Gatti *et al.* applied GW + cumulant expansion to $SrVO_3$ and obtained improved spectra for the upper Hubbard band [28]. Moreover, as the GW calculation in this work is done

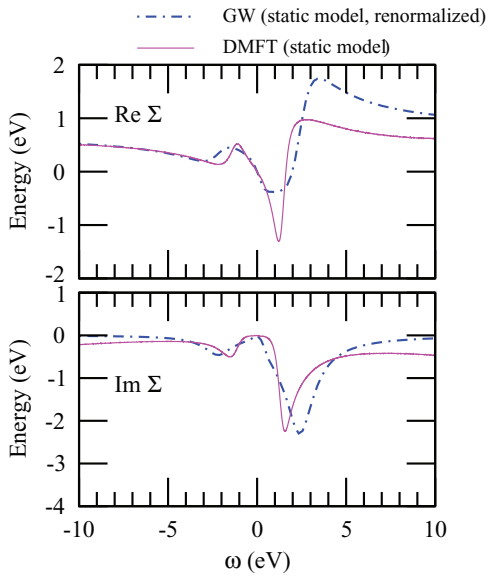

FIG. 10. (Color online) Self-energy of $SrVO_3$ in the static model calculated with the GWA and DMFT. The GW self-energy is calculated from the band structure whose bandwidth is renormalized by 0.5 from the LDA.

non-self-consistently starting from the LDA eigenstates, another source of discrepancies between the DMFT and GW results may be due to the inaccurate initial states (i.e., LDA Kohn-Sham states) in the GWA calculation. To highlight this effect, in Fig. 10 we plot the result of the static model calculation within the GWA for $SrVO_3$ by scaling the starting one-particle bandwidth by 0.5, which yields approximately the bandwidth given by the DMFT calculation. The positions of the two peaks in Im $\Sigma(\omega)$ become closer to $\omega = 0$ while they are still larger than the DMFT ones. We get similar results for Fe, but the non-Fermi-liquid behavior remains missing, since it is a consequence of local correlations beyond the description within the GWA. The effects of both the vertex correction and the self-consistency are important ingredients to understand if we want to perform a more "quantitative" comparison between DMFT and the GWA in a future study.

V. SUMMARY AND CONCLUSIONS

Focusing on the $3d$ band of Fe and the t_{2g} band of $SrVO_3$, we have performed three types of detailed GW calculations: *ab initio*, dynamic model, and static model calculations. In contrast to the static model, the dynamic model takes into account the frequency dependence of U but both models employ a local on-site interaction U. The *ab initio* calculations take into account both the frequency dependence and intersite components of U as well as the exchange and correlation between the r and d states [i.e., Σ^{rd} in Eq. (2)]. They may be regarded as the "exact" results in this study and serve as a benchmark for comparison. The main outcome is displayed in Fig. 7 and Table I, from which the following conclusions can be reached: (1) The difference in the bandwidth between the *ab initio* and dynamic model quasiparticle band structures is due to the **k** dependence of the self-energy that is essentially missing in the dynamic model which includes only the d electrons and an on-site interaction. The local character of the dynamic model self-energy can be seen in Figs. 5 and 6 in which little difference is found between the dynamic model self-energy and the local component of the d contribution of the GW self-energy. Further evidence may be found in Table I where the renormalization factors of the dynamic model are close to those of the local GW. Our comparison between the model and *ab initio* self-energies shows that this **k**-dependent component of the self-energy mainly arises from both the nonlocal component of $U(\omega)$ and the correlation between r and d electrons [Σ^{rd} in Eq. (2)] rather than from G_0^d. Moreover, this **k** dependence tends to widen the bandwidth, consistent with previous findings [13]. In other words, a dynamic model with on-site interaction only tends to overestimate the band renormalization. (2) A new and unexpected result is found for the static model. Although the static model neglects both frequency dependence of U and intersite U, the quasiparticle band structure shows a better agreement with the *ab initio* result than the dynamic model, as may be seen in Fig. 7. The reason for this can be traced back to a strong cancellation between the effects of the frequency dependence and nonlocal U. Frequency-dependent U increases correlation effects as reflected in increased band renormalization, whereas nonlocal or intersite U tends to widen the bandwidth. This cancellation between the effects of the frequency dependence and nonlocal U is in a way fortuitous but on the other hand it provides a theoretical justification for the static model although a proper and accurate model should include both frequency dependence and nonlocal U as shown in a recent work [67].

We have also made a comparison between the self-energy in the GWA and DMFT for the static model of these two systems. A non-Fermi-liquid behavior of paramagnetic Fe and some Hubbard satellites of $SrVO_3$ are reported in DMFT but are missing in the GWA because they are consequences of the local correlations. This prevents from any general quantitative comparison of the satellites in the self-energies and of the bandwidth reduction within these two approaches. However, a larger renormalization due to the dynamic screening is reported in recent DMFT calculations with frequency-dependent interactions by Casula *et al.* and Werner *et al.* [6,7]. This suggests that the effects of the frequency dependence and nonlocal U compensate each other in the static model within the DMFT framework too. It would be interesting to compare the dynamic and static models within DMFT for strongly correlated systems, especially for paramagnetic Fe, to study any effects of frequency dependence and intersite U on its non-Fermi-liquid behavior.

Our findings motivate us to develop a method for realistic calculations such as the GW + (extended) DMFT method [68–71] which incorporates strong local correlations between d electrons with the full (i.e., frequency-dependent and long-range) screened interaction U, as well as the correlations between the correlated d electrons and r electrons missing in usual effective models. Work along this direction is on its way.

ACKNOWLEDGMENTS

This work was supported by the Swedish Research Council. T.M. acknowledges the support from HPCI Strategic Programs

for Innovative Research (SPIRE), CMSI, and by KAKENHI (Grant No. 22104010) from MEXT, Japan. R.S. also acknowledges the support from the Scandinavia-Japan Sasakawa Foundation.

APPENDIX: REDUCED INTERACTION MATRICES IN DMFT

Here we list the values of the reduced interaction matrices used in our DMFT calculations. For the t_{2g} orbitals of $SrVO_3$, there is a direct correspondence between the Hubbard-Kanamori parameters and the static values of the effective interaction $U(\omega = 0)$ obtained in the GW calculation:

$$\begin{aligned} \mathcal{U} &= U^{\sigma\bar{\sigma}}_{mm} = 3.40 \text{ eV}, \\ \mathcal{J} &= J_{mm'} = 0.47 \text{ eV}, \quad m \neq m'. \end{aligned} \tag{A1}$$

From these values, one obtains the following interaction matrices:

$$U^{\sigma\sigma}_{mm'}(\mathrm{SrVO_3}) = \begin{pmatrix} 0.00 & 2.00 & 2.00 \\ 2.00 & 0.00 & 2.00 \\ 2.00 & 2.00 & 0.00 \end{pmatrix}, \tag{A2}$$

$$U^{\sigma\bar{\sigma}}_{mm'}(\mathrm{SrVO_3}) = \begin{pmatrix} 3.40 & 2.47 & 2.47 \\ 2.47 & 3.40 & 2.47 \\ 2.47 & 2.47 & 3.40 \end{pmatrix}. \tag{A3}$$

The ordering of the orbitals in these matrices is d_{xy}, d_{xz}, and d_{yz}. The values are given in eV. In these expressions, $U^{\sigma\bar{\sigma}}_{mm'}$ for $m \neq m'$ is obtained by the relation $\mathcal{U} - 2\mathcal{J} = 2.47$ eV induced by the cubic symmetry of the system. For comparison, the direct extraction of these matrix elements from the static values of the effective interaction $U(\omega = 0)$ gives the value

$$U^{\sigma\bar{\sigma}}_{mm'} = 2.42 \text{ eV}, \quad m \neq m'. \tag{A4}$$

The discrepancy of 2% comes from the deviation of the Wannier functions from the atomic t_{2g} orbitals.

For the d orbitals of paramagnetic Fe, we find $\mathcal{U} = 3.37$ eV and $\mathcal{J} = 0.97$ eV, where $\mathcal{U}$ and $\mathcal{J}$ are related to the Slater integrals thanks to the formulas given in Eq. (30). From these values, the interaction matrices are the following:

$$U^{\sigma\sigma}_{mm'}(\mathrm{Fe}) = \begin{pmatrix} 0.00 & 1.90 & 1.90 & 2.90 & 2.90 \\ 1.90 & 0.00 & 3.23 & 2.23 & 2.23 \\ 1.90 & 3.23 & 0.00 & 2.23 & 2.23 \\ 2.90 & 2.23 & 2.23 & 0.00 & 2.23 \\ 2.90 & 2.23 & 2.23 & 2.23 & 0.00 \end{pmatrix}, \tag{A5}$$

$$U^{\sigma\bar{\sigma}}_{mm'}(\mathrm{Fe}) = \begin{pmatrix} 4.48 & 2.76 & 2.76 & 3.42 & 3.42 \\ 2.76 & 4.48 & 3.65 & 2.98 & 2.98 \\ 2.76 & 3.65 & 4.48 & 2.98 & 2.98 \\ 3.42 & 2.98 & 2.98 & 4.48 & 2.98 \\ 3.42 & 2.98 & 2.98 & 2.98 & 4.48 \end{pmatrix}. \tag{A6}$$

The ordering of the orbitals in these matrices is $d_{3z^2-r^2}$, $d_{x^2-y^2}$, d_{xy}, d_{xz}, and d_{yz}. The values are given in eV. For comparison, the static values of the effective interaction $U(\omega = 0)$ obtained in the GW calculation are given below, with the same ordering of the orbitals:

$$J_{mm'}(\mathrm{Fe}) = \begin{pmatrix} 0.00 & 0.86 & 0.82 & 0.53 & 0.53 \\ 0.86 & 0.00 & 0.43 & 0.72 & 0.72 \\ 0.82 & 0.43 & 0.00 & 0.70 & 0.70 \\ 0.53 & 0.72 & 0.70 & 0.00 & 0.70 \\ 0.53 & 0.72 & 0.70 & 0.70 & 0.00 \end{pmatrix}, \tag{A7}$$

$$U^{\sigma\bar{\sigma}}_{mm'}(\mathrm{Fe}) = \begin{pmatrix} 4.62 & 2.91 & 2.82 & 3.41 & 3.41 \\ 2.91 & 4.62 & 3.61 & 3.02 & 3.02 \\ 2.82 & 3.61 & 4.32 & 2.92 & 2.92 \\ 3.41 & 3.02 & 2.92 & 4.32 & 2.92 \\ 3.41 & 3.02 & 2.92 & 2.92 & 4.32 \end{pmatrix}. \tag{A8}$$

The discrepancies observed between the parametrized matrices and the calculated values of $U(\omega = 0)$ within constrained RPA may introduce small quantitative differences in the features observed in the self-energy but are not expected to modify its general behavior discussed in this work.

[1] A. Georges, G. Kotliar, W. Krauth, and M. J. Rozenberg, Rev. Mod. Phys. **68**, 13 (1996).
[2] V. I. Anisimov, A. I. Poteryaev, M. A. Korotin, A. O. Anokhin, and G. Kotliar, J. Phys.: Condens. Matter **9**, 7359 (1997).
[3] A. I. Lichtenstein and M. I. Katsnelson, Phys. Rev. B **57**, 6884 (1998).
[4] G. Kotliar, S. Y. Savrasov, K. Haule, V. S. Oudovenko, O. Parcollet, and C. A. Marianetti, Rev. Mod. Phys. **78**, 865 (2006).
[5] F. Aryasetiawan, M. Imada, A. Georges, G. Kotliar, S. Biermann, and A. I. Lichtenstein, Phys. Rev. B **70**, 195104 (2004).
[6] M. Casula, Ph. Werner, L. Vaugier, F. Aryasetiawan, T. Miyake, A. J. Millis, and S. Biermann, Phys. Rev. Lett. **109**, 126408 (2012).
[7] P. Werner, M. Casula, T. Miyake, F. Aryasetiawan, A. J. Millis, and S. Biermann, Nat. Phys. **8**, 331 (2012).
[8] L. Huang and Y. Wang, Europhys. Lett. **99**, 67003 (2012).
[9] P. Werner and A. J. Millis, Phys. Rev. Lett. **99**, 146404 (2007).
[10] P. Werner and A. J. Millis, Phys. Rev. Lett. **104**, 146401 (2010).
[11] M. Casula, A. Rubtsov, and S. Biermann, Phys. Rev. B **85**, 035115 (2012).
[12] J. M. Tomczak, M. van Schilfgaarde, and G. Kotliar, Phys. Rev. Lett. **109**, 237010 (2012).
[13] T. Miyake, C. Martins, R. Sakuma, and F. Aryasetiawan, Phys. Rev. B **87**, 115110 (2013).
[14] L. Hedin, Phys. Rev. **139**, A796 (1965).
[15] F. Aryasetiawan and O. Gunnarsson, Rep. Prog. Phys. **61**, 237 (1998).
[16] W. G. Aulbur, L. Jönsson, and J. W. Wilkins, Solid State Phys. **54**, 1 (1999).

[17] A. I. Lichtenstein, M. I. Katsnelson, and G. Kotliar, Phys. Rev. Lett. **87**, 067205 (2001).

[18] K. Maiti, D. D. Sarma, M. J. Rozenberg, I. H. Inoue, H. Makino, O. Goto, M. Pedio, and R. Cimino, Europhys. Lett. **55**, 246 (2001).

[19] A. Liebsch, Phys. Rev. Lett. **90**, 096401 (2003).

[20] K. Maiti, U. Manju, S. Ray, P. Mahadevan, I. H. Inoue, C. Carbone, and D. D. Sarma, Phys. Rev. B **73**, 052508 (2006).

[21] A. A. Katanin, A. I. Poteryaev, A. V. Efremov, A. O. Shorikov, S. L. Skornyakov, M. A. Korotin, and V. I. Anisimov, Phys. Rev. B **81**, 045117 (2010).

[22] I. Leonov, A. I. Poteryaev, V. I. Anisimov, and D. Vollhardt, Phys. Rev. Lett. **106**, 106405 (2011).

[23] V. I. Anisimov, A. S. Belozerov, A. I. Poteryaev, and I. Leonov, Phys. Rev. B **86**, 035152 (2012).

[24] I. A. Nekrasov, K. Held, G. Keller, D. E. Kondakov, Th. Pruschke, M. Kollar, O. K. Andersen, V. I. Anisimov, and D. Vollhardt, Phys. Rev. B **73**, 155112 (2006).

[25] B. Amadon, F. Lechermann, A. Georges, F. Jollet, T. O. Wehling, and A. I. Lichtenstein, Phys. Rev. B **77**, 205112 (2008).

[26] J. M. Tomczak, M. Casula, T. Miyake, F. Aryasetiawan, and S. Biermann, Europhys. Lett. **100**, 67001 (2012).

[27] C. Taranto, M. Kaltak, N. Parragh, G. Sangiovanni, G. Kresse, A. Toschi, and K. Held, Phys. Rev. B **88**, 165119 (2013).

[28] M. Gatti and M. Guzzo, Phys. Rev. B **87**, 155147 (2013).

[29] F. Aryasetiawan, J. M. Tomczak, T. Miyake, and R. Sakuma, Phys. Rev. Lett. **102**, 176402 (2009).

[30] R. M. Dreizler and E. K. U. Gross, *Density Functional Theory* (Springer-Verlag, Berlin, 1990).

[31] F. Aryasetiawan, K. Karlsson, O. Jepsen, and U. Schönberger, Phys. Rev. B **74**, 125106 (2006).

[32] T. Miyake and F. Aryasetiawan, Phys. Rev. B **77**, 085122 (2008).

[33] T. Miyake, F. Aryasetiawan, and M. Imada, Phys. Rev. B **80**, 155134 (2009).

[34] J. Negele and H. Orland, *Quantum Many-Particle Systems* (Perseus Books, New York, 1988).

[35] We define Re $A = \frac{A+A^\dagger}{2}$ and Im $A = \frac{A-A^\dagger}{2i}$.

[36] F. Aryasetiawan, Phys. Rev. B **46**, 13051 (1992).

[37] L. Vaugier, H. Jiang, and S. Biermann, Phys. Rev. B **86**, 165105 (2012).

[38] This should not be confused with the spatial locality of the self-energy; even in DMFT the self-energy is nonlocal in real-space representation [i.e., $\Sigma(\mathbf{r},\mathbf{r}') \neq \delta(\mathbf{r}-\mathbf{r}')\Sigma(\mathbf{r},\mathbf{r})$].

[39] See http://www.flapw.de/.

[40] C. Friedrich, S. Blügel, and A. Schindlmayr, Phys. Rev. B **81**, 125102 (2010).

[41] J. P. Perdew and A. Zunger, Phys. Rev. B **23**, 5048 (1981).

[42] N. Marzari and D. Vanderbilt, Phys. Rev. B **56**, 12847 (1997).

[43] I. Souza, N. Marzari, and D. Vanderbilt, Phys. Rev. B **65**, 035109 (2001).

[44] N. Marzari, A. A. Mostofi, J. R. Yates, I. Souza, and D. Vanderbilt, Rev. Mod. Phys. **84**, 1419 (2012).

[45] R. Sakuma, Phys. Rev. B **87**, 235109 (2013).

[46] A. A. Mostofi, J. R. Yates, Y.-S. Lee, I. Souza, D. Vanderbilt, and N. Marzari, Comput. Phys. Commun. **178**, 685 (2008).

[47] L. Hedin, J. Phys.: Condens. Matter **11**, R489 (1999).

[48] I. V. Solovyev and M. Imada, Phys. Rev. B **71**, 045103 (2005).

[49] D. R. Hamann and D. Vanderbilt, Phys. Rev. B **79**, 045109 (2009).

[50] M. Ferrero and O. Parcollet, *TRIQS: A Toolbox for Research in Interacting Quantum Systems*, http://ipht.cea.fr/triqs.

[51] P. Blaha, K. Schwarz, G. Madsen, D. Kvasnicka, and J. Luitz, *WIEN2k, An Augmented Plane Wave+Local Orbitals Program for Calculating Crystal Properties* (Technische Universitat Wien, Austria, 2009).

[52] M. Aichhorn, L. Pourovskii, V. Vildosola, M. Ferrero, O. Parcollet, T. Miyake, A. Georges, and S. Biermann, Phys. Rev. B **80**, 085101 (2009).

[53] To minimize this entanglement, we use an energy window from −5 to 4 eV to build the Wannier functions in our calculation for Fe.

[54] P. Werner, A. Comanac, L. de' Medici, M. Troyer, and A. J. Millis, Phys. Rev. Lett. **97**, 076405 (2006)

[55] We perform a DMFT calculation with the full interaction matrix for $SrVO_3$. Taking into account the nondensity-density terms does not significantly modify the results for this material. On the contrary, for Fe, the nondensity-density terms in the Coulomb vertex dramatically increase the computational cost of CTQMC, preventing us from reaching results accurate enough.

[56] I. Solovyev, J. Phys. Soc. Jpn. **78**, 054710 (2009).

[57] I. Solovyev, J. Phys.: Condens. Matter **20**, 293201 (2008).

[58] V. I. Anisimov, I. V. Solovyev, M. A. Korotin, M. T. Czyzyk, and G. A. Sawatzky, Phys. Rev. B **48**, 16929 (1993).

[59] V. I. Anisimov, J. Zaanen, and O. K. Andersen, Phys. Rev. B **44**, 943 (1991).

[60] K. S. D. Beach, arXiv:cond-mat/0403055.

[61] T. Yoshida, M. Hashimoto, T. Takizawa, A. Fujimori, M. Kubota, K. Ono, and H. Eisaki, Phys. Rev. B **82**, 085119 (2010).

[62] F. Aryasetiawan, L. Hedin, and K. Karlsson, Phys. Rev. Lett. **77**, 2268 (1996).

[63] M. Guzzo, G. Lani, F. Sottile, P. Romaniello, M. Gatti, J. J. Kas, J. J. Rehr, M. G. Silly, F. Sirotti, and L. Reining, Phys. Rev. Lett. **107**, 166401 (2011).

[64] M. Gatti, F. Bruneval, V. Olevano, and L. Reining, Phys. Rev. Lett. **99**, 266402 (2007).

[65] R. Sakuma, T. Miyake, and F. Aryasetiawan, Phys. Rev. B **78**, 075106 (2008).

[66] R. Sakuma, T. Miyake, and F. Aryasetiawan, Phys. Rev. B **86**, 245126 (2012).

[67] R. Sakuma, Ph. Werner, and F. Aryasetiawan, Phys. Rev. B **88**, 235110 (2013).

[68] S. Biermann, F. Aryasetiawan, and A. Georges, Phys. Rev. Lett. **90**, 086402 (2003).

[69] T. Ayral, Ph. Werner, and S. Biermann, Phys. Rev. Lett. **109**, 226401 (2012).

[70] T. Ayral, S. Biermann, and Ph. Werner, Phys. Rev. B **87**, 125149 (2013).

[71] L. Huang, T. Ayral, S. Biermann, and Ph. Werner, arXiv:1404.7047.